THE JOURNAL OF PHYSICAL CHEMISTRY C

Article

pubs.acs.org/JPCC

Surface Decoration of MgO Nanocubes with Sulfur Oxides: Experiment and Theory

Andreas Sternig and Oliver Diwald*

Institute of Particle Technology, Friedrich-Alexander University Erlangen-Nürnberg,, Cauerstraße 4, 91058 Erlangen, Germany

Silvia Gross

Istituto di Scienze e Tecnologie Molecolari, ISTM-CNR, Dipartimento di Scienze Chimiche, Università degli Studi di Padova, and INSTM, via Marzolo, 1, I-35131, Padova, Italy

Peter V. Sushko*

University College London, Department of Physics and Astronomy, London WC1E 6BT, United Kingdom

ABSTRACT: We investigated the effect of surface sulfate formation on the structure and spectroscopic properties of MgO nanocubes using X-ray diffraction, electron microscopy, several spectroscopic techniques, and ab initio calculations. After CS_2 adsorption and oxidative treatment at elevated temperatures the MgO particles remain cubic and retain their average size of ~6 nm. Their low coordinated surface elements (corners and edges) were found to bind sulfite and sulfate groups even after annealing up to 1173 K. The absence of MgO corner specific photoluminescence emission bands at 3.4 and 3.2 eV substantiates that sulfur modifies the electronic properties of characteristic surface structures, which we attribute to the formation of $(SO_3)^{2-}$ and $(SO_4)^{2-}$ groups at corners and edges. Ab initio calculations support these conclusions and provide insight into the local atomic structures and spectroscopic properties of these groups.

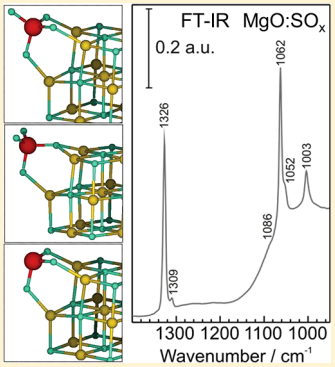

1. INTRODUCTION

Oxides with pronounced surface basicity, such as those of the alkaline earth metals, are utilized as adsorbents for the removal of acidic gases from combustion emission.[1] Moreover, sulfur oxides and carbonyl sulfides (COS) are abundant aerosols in the troposphere where they participate in many heterogeneous reactions. For these reasons, their interaction with mineral oxides has received great attention in environmental science and technology.[2−5] From the perspective of the synthesis and functionalization of nanomaterials, a lot of effort is directed at the controlled modification of oxide surfaces via decoration of selected surface elements with atoms and molecules. Surface adsorbates can induce local electronic structure changes and give rise to interesting new functionalities. The corresponding adjustment of surface reactivity[6] and surface optical properties[7−10] requires understanding of the underlying adsorption processes.[11] In a recent study by Scarano et al.,[12] the interaction of CS_2 with polycrystalline MgO was comprehensively explored using FT-IR and UV−Vis spectroscopies in combination with ab initio electronic structure calculations. The authors addressed the reactivity of low coordinated (LC) surface elements, such as corners and kinks toward CS_2. As a major result, they found that CS_2 adsorption transforms the reactive polycrystalline material into a chemically inert system. Surface anions located on MgO edges and corners react with CS_2 in a way that is similar to that found for CO_2 activation:[13−15]

$$O_{LC}{}^{2-}—Mg^{2+}—O_{LC}{}^{2-} + CS_2 \rightarrow O_{LC}{}^{2-}—Mg^{2+}—[OCS_2]^{2-} \quad (1)$$

$$O_{LC}{}^{2-}—Mg^{2+}—[OCS_2]^{2-} \rightarrow S_{LC}{}^{2-}—Mg^{2+}—[OCOS]^{2-} \quad (2)$$

Adsorbed $[OCS_2]^{2-}$, $[OCOS]^{2-}$, and $[OCO_2]^{2-}$ moieties exhibit multidentate binding modes. In addition to the FT-IR study which addressed the reaction steps described in eqs 1 and 2 at room temperature, it was found that $[OCS_2]^{2-}$ and $[OCOS]^{2-}$ species decompose above room temperature and, in the course of this process, S^{2-} ions substitute low coordinated O^{2-} sites.[12] Using electron paramagnetic resonance spectroscopy (EPR) Livraghi et al.[5] studied CS_2 interaction with electron-rich MgO surfaces and identified CS_2^- as anionic radicals together with paramagnetic sulfur S_n^- oligomers (with $n = 1$ and ≥ 3) of limited thermal stability. Thus, after annealing in vacuum the overall chemical reaction between adsorbed CS_2

Received: February 8, 2013
Revised: March 15, 2013
Published: March 21, 2013

   dx.doi.org/10.1021/jp401432j | J. Phys. Chem. C 2013, 117, 7727−7735

molecules and MgO surfaces is expected to lead to S-doped MgO surfaces, MgO(S):

$$MgO + CS_2 \rightarrow MgO(S) + COS \quad (3)$$

The exchange of ions between nanostructured surfaces and those originating from gas phase molecules[14,15] carry high potential for surface functionalization. We are interested in exploiting these reactions in order to modify MgO nanocubes. These exhibit a high concentration of low index (001) facets that are framed by 4-fold coordinated (4C) ions at edges and 3-fold coordinated ions (3C) at corners.[16,7] A variety of spectroscopic techniques[17−21] as well as first-principles theoretical calculations[22−26] have been used to characterize the electronic properties of related particle powders. UV diffuse reflectance spectroscopy reveals two absorption bands below the bulk absorption threshold of MgO, which are attributed to corner (4.6 eV) and edge sites (5.2 eV). Photoluminescence (PL) spectroscopy detects two closely spaced emission bands at 3.4 and 3.2 eV, which result from photoexcitation of edges and corners, respectively.[17,27,28] Thus, MgO nanocubes represent a well characterized model system that is useful to explore adsorption and ion exchange reactions at particle surfaces. Corresponding insights may be transferable to those obtained on single crystalline model surfaces investigated under ultrahigh vacuum.[29−34]

In the present study, we explored the possibility of exchanging surface O^{2-} in MgO nanocubes with S^{2-} via CS_2 adsorption and investigated the thermal stability and spectroscopic properties of the resulting species. Different from sample treatment procedures in non oxidizing atmospheres where neutral and anionic sulfur species prevail,[5,12] we applied CS_2 adsorption in combination with high temperature oxidation and subsequent vacuum annealing. The activation procedure was chosen to address the impact of thermally stable adsorbates on the surface electronic structure. Our main conclusion is that sulfites $[SO_3]^{2-}$ and sulfates $[SO_4]^{2-}$ form in the process of the surface treatment and remain dominating surface groups on MgO nanocube after annealing to 1173 K.

2. METHODS

2.1. Nanocrystal Synthesis and CS_2 Adsorption. For the production of MgO nanoparticles, we use a chemical vapor synthesis (CVS) procedure corresponding to the controlled evaporation and subsequent oxidation of alkaline earth metals under reduced pressure.[35] Stable processing conditions are provided by spatially separating the evaporation and oxidation zones. The reactor system employed consists of two quartz glass tubes, which are placed inside a cylindrical furnace. The inner tube hosts ceramic ships with Mg grains (99.98%, Aldrich), which are heated to 913 K to ensure a sufficiently high metal vapor pressure. An inert argon stream transports the metal vapor away from the evaporation zone to the end of the inner glass tube where the metal vapor meets the oxidizing agent coming from the outer glass tube. The exothermic oxidation reaction leads to a bright stable flame in the oxidation zone of the reactor and MgO nanoparticles are formed as a result of homogeneous nucleation in the gas phase. Because of continuous pumping, the residence time of nuclei within the flame is <2 ms, which prevents substantial coarsening and coalescence. A bypass system ensures nanoparticle collection only during the time of controlled process conditions (i.e., temperature, pressure, and flow rate). The total pressure in the CVS-reactor is kept constant at 50 ± 3 mbar over the entire production process. After production, the MgO nanoparticles powder is transferred into quartz glass cells, which allows one to perform thermal activation of the nanoparticle powders in defined gas atmospheres. To obtain well-defined cubic MgO nanoparticles, the organic contamination of the as-obtained MgO powder is removed by heating to 1123 K at a rate of 5 $K \cdot min^{-1}$ and exposing to molecular oxygen (10 mbar) at this temperature. Then, the sample temperature is raised to 1173 K at pressures $p < 5 \times 10^{-6}$ mbar and kept at this temperature for 1 h.

Prior to adsorption of CS_2 on MgO nanocubes, the CS_2 is cleaned employing the freeze−pump−thaw method. The adsorption experiments are carried out at a base pressure of 3×10^{-5}mbar using the setup shown in Figure 1. In a typical

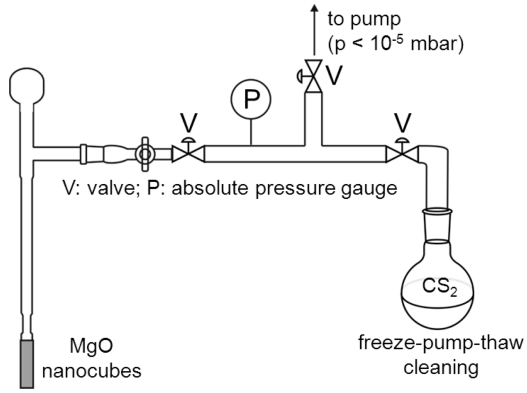

Figure 1. Scheme illustrating the set up for MgO nanocubes annealing and subsequent CS_2 adsorption at room temperature.

experiment MgO nanocubes are exposed to a partial pressure of 60 mbar CS_2 for a typical exposure time of 10 s.[36] Then, the powder inside the quartz glass cuvette is evacuated to $p < 5 \times 10^{-6}$ mbar and subjected to a procedure that is identical to that applied to the as-obtained powder. The structural and optical properties of the as-treated sample (hereafter called MgO:SO_x) are compared to those of pure MgO nanocubes.

2.2. Structure and Morphology. X-ray diffraction patterns were collected on a PANalytical X'Pert PRO diffractometer using Cu K_α radiation. The average nanocrystal sizes were derived on the basis of the Scherrer equation with the assumption of cubically shaped nanocrystals. We used pseudo-Voigt functions to determine the full width at half-maximum of the three main reflexes to calculate an average nanocrystal size (d_{XRD}). Small amounts of the metal oxide powders were cast on a holey carbon grid for investigation with a TECNAI F20 analytical TEM equipped with a field emission gun and a S-twin objective lens.

2.3. Spectroscopy. X-ray photoelectron spectroscopy (XPS) measurements were carried out on a Perkin-Elmer Φ5600ci spectrometer using standard Al radiation (1486.6 eV) working at 300 W. Prior to the measurements, MgO and MgO:SO_x powder samples, which had been subjected to vacuum annealing and oxygen treatment at elevated temperatures as described above, were transferred to the XPS spectrometer system in dedicated vacuum cells. The vacuum of the cells was broken immediately before sample introduction into the XPS analytical chamber. Exposure of the samples to air for approximately 30 min between breaking the vacuum of the cell, sample mounting and its transfer into the load lock was inevitable. The working pressure of the XPS system was $p < 5 \times$

dx.doi.org/10.1021/jp401432j | J. Phys. Chem. C 2013, 117, 7727−7735

10^{-9} mbar. The spectrometer was calibrated by assuming the binding energy (BE) of the $Au4f_{7/2}$ line at 83.9 eV with respect to the Fermi level. The standard deviation for the binding energy values was 0.15 eV. The reported binding energies were corrected for charging effects with respect to the 1s line of carbon, which has a BE of 284.6 eV.[37,38] Survey scans (187.85 pass energy, 1 eV/step, 25 ms per step) were obtained in the 0−1300 eV range. Detailed scans (58.7 eV pass energy, 1 eV/step, 25 ms per step) were recorded for the O1s, C1s, Mg2p, Mg1s, MgKLL, S2p, and S2s regions. Peak assignments were carried out using the values reported in the *Handbook of X-ray Photoelectron Spectroscopy*[37] and in the NIST XPS database,[39] as well as in the quoted references.

The IR experiments were performed in a cell that allows for sample activation at high-vacuum conditions with a base pressure below 5×10^{-6} mbar. Samples in the form of hand-pressed, self-supporting pellets were measured in the IR transmission mode with a Bruker 113v spectrometer. A total of 300 scans were accumulated for one spectrum to obtain a reasonable signal-to-noise ratio with a spectral resolution of 3 cm^{-1}.

Photoluminescence and UV diffuse reflectance measurements were carried out at room temperature; the samples were contained within the quartz glass cells that guarantee vacuum conditions better than $p = 5 \times 10^{-6}$ mbar. UV diffuse reflectance spectra were acquired using a Perkin-Elmer Lambda 750 spectrophotometer equipped with an integrating sphere and then converted to absorption spectra by the Kubelka−Munk transform procedure. Diffuse reflectance measurements were carried out in the presence of 10 mbar O_2 to quench potential surface photoluminescence emission effects, which would generate false positive deviations from the true reflectance values. Photoluminescence spectra were measured on an Edinburgh Instruments spectrometer system FSP920 using a CW 450 W Xenon arc lamp for excitation. The basic architecture of an Edinburgh Instruments spectrometer has the emission and excitation arms orientated around the sample chamber in an L-geometry. The spectrometer is equipped with a double monochromator on the emission and excitation side to guarantee optimal stray light rejection.

2.4. Theoretical Modeling. The experimental data were supported by ab initio calculations carried out using an embedded cluster approach. In brief, an MgO nanoparticle was modeled by a cube of $20 \times 20 \times 20$ atoms terminated with (001) atomic planes. An oxygen-terminated corner of this particle was modeled quantum-mechanically (QM) using a $Mg_{13}O_{13}$ cluster embedded in the potential produced by the remaining part of the nanoparticle, which was represented using the classical shell model. The cations at the interface between the QM and the shell model regions were represented using the full ion potentials.[40] Formal ionic charges were used. The details of this method are described elsewhere.[41,42] Oxygen and Mg atoms of the QM cluster were represented using 6-311G* basis sets. The QM contribution to the total energy were calculated using the hybrid density functional B3LYP,[43,44] as implemented in the Gaussian 03 package.[45] The excitation energies (ε) and the corresponding oscillator strengths (f) were calculated using the time-dependent DFT method[46] and the B3LYP density functional. The optical absorption spectra were then simulated as a convolution of functions $g(\varepsilon) = f_n \times \exp[(\varepsilon - \varepsilon_n)^2/a^2]$ (n = 1−35) for the lowest-energy transitions. The constant a was selected so that the full width at half of the maximum of $g(\varepsilon)$ was 0.2 eV. Vibrational frequencies were calculated by numerically differentiating the total energy with respect to the coordinates of selected atoms.

3. RESULTS AND DISCUSSION

3.1. Structure and Morphology. CS_2 adsorption on MgO nanocubes and subsequent high temperature treatment do neither affect the cubic morphology specific to the MgO nanocubes nor their average particle size (Figure 2a and b).

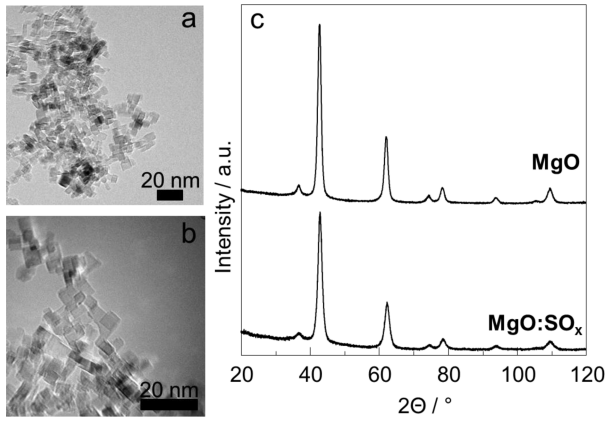

Figure 2. TEM images of $MgO:SO_x$ powders after oxidation (a) and vacuum annealing at 1173 K (b), demonstrating that the cubic morphology is retained. (c) XRD powder patterns of MgO and $MgO:SO_x$ reveal that both powders crystallize in the cubic rock salt phase.

XRD confirms that both powders, MgO and $MgO:SO_x$, crystallize in the cubic rock salt phase (Figure 2c). XRD reflections related to magnesium−sulfur compounds such as MgS, $MgSO_3$, and $MgSO_4$ were not observed. Using the Scherrer equation, the average crystallite size was estimated from reflex broadening in XRD powder patterns.[47,48] Domain sizes of 6.5 nm ±1.0 nm were derived for MgO and $MgO:SO_x$ nanocube powders.

3.2. Surface Composition. The surface composition of the samples was analyzed by XPS. The XPS survey spectrum of a $MgO:SO_x$ sample (Figure 3a) reveals the presence of Mg and O, whereas the additional presence of carbon is attributed to surface organic contaminations because of the sample exposure to the atmosphere in the time interval between breaking the vacuum of the transfer cell, sample mounting and transfer into the load lock of the XPS system ($t \approx 30$ min). A survey spectrum of MgO nanocubes (not shown) without prior

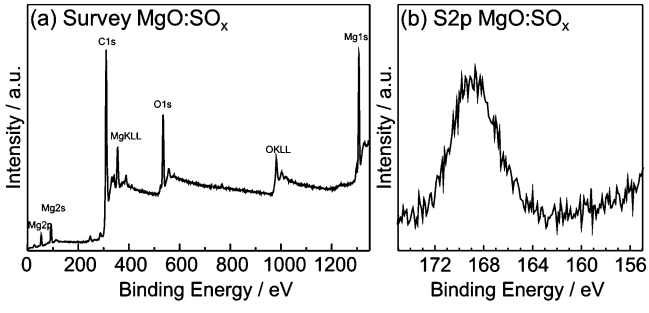

Figure 3. XPS survey spectrum (a) and selected area spectrum of the S2p region (b) of $MgO:SO_x$ powders, which were obtained after oxidation and vacuum annealing of MgO nanoparticles with adsorbed CS_2.

dx.doi.org/10.1021/jp401432j | J. Phys. Chem. C 2013, 117, 7727−7735

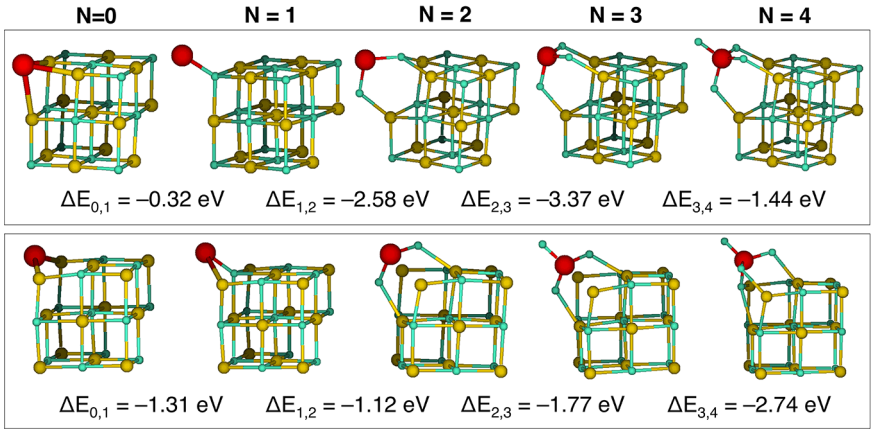

Figure 4. Geometrical configurations of SO_x complexes at the 3-coordinated (top) and 4-coordinated (bottom) surface sites of MgO nanocubes. Oxygen, magnesium, and sulfur atoms are shown using small (blue), medium (yellow), and large (red) spheres, respectively. Energy changes are calculated with respect to 1/2 of the O_2 molecule.

contact with CS_2 revealed identical signals related to Mg, O, and C with comparable peak intensities. Because of its low concentration, sulfur could be evidenced only by selected area scans covering the S2p region (155−175 eV). Exclusively in the case of the MgO:SO_x sample, a significant spectral feature with a binding energy of about 169 eV was observed (Figure 3b). We attribute this feature to sulfur in a positive oxidation state, such as in sulfite (SO_3^{2-}) and sulfate (SO_4^{2-}) groups, reported in the literature to peak in the energy ranges 165.6−167.0 and 168.0−170.1 eV, respectively.[37,49,13] The broadening of the peak (FWHM of about 5 eV) hints at the presence of sulfur in slightly different chemical environments, for instance to the copresence of sulfite and sulfate anions. No characteristic XPS features ascribable to sulfide ions (S^{2-})[37] have been found in the binding energy range between 160.0 and 162.5 eV (Figure 3b), which are typical of sulfide species. The presence of pure CS_2, whose S2p region would be characterized by a binding energy of 163.6 eV could also be ruled out.[37] Taken together, our results suggest that the process of CS_2 adsorption on MgO nanocubes followed by subsequent oxidation and vacuum annealing yields sulfite $(SO_3)^{2-}$ or sulfate $(SO_4)^{2-}$ surface groups rather than S^{2-}, which would substitute surface oxygen anions. No sulfur specific XPS signal was observed for pure, that is, untreated with sulfur MgO nanocubes (spectrum not shown), as expected.

3.3. Prediction of Surface Structures. To get further insights into the relative stability of S-containing surface species and associated structures, we performed ab initio calculations of SO_x surface species. It was assumed that high temperature oxidation eliminates all carbon that would originate from CS_2 adsorption. Because of the presence of oxygen at elevated temperatures, we expect that surface SO_x species acquire as much oxygen as required to maximize their thermodynamic stability. Finally, for the sake of simplicity, we only considered isolated sulfur species at low coordinated surface sites, which are known to be most reactive. To this end, we defined a reference configuration, in which an S atom occupies a surface O site and then considered the variety of the structures formed by addition of $N/2$ oxygen molecules. The lowest-energy configurations for N = 0−4 are shown in Figure 4.

The top panel shows the structures originating from a reference configuration, in which an S atom occupies a 3-coordinated oxygen site. The values of the energy gain associated with the addition of 1/2 O_2 for each N suggest that substitutional S atoms can exist as transient species in an oxygen-poor atmosphere only. Once oxygen is supplied, the local atomic structure of the corner site changes so as oxidation state of the S atom increases from −2 (N = 0) to +6 (N = 4). Each change of the oxidation state can be associated with either (i) consecutive attachment of O atoms or (ii) dissociation of an O_2 molecules and attachment of the two O atoms simultaneously. The latter is possible if the energy gain because of attachment of two O atoms exceeds the dissociation energy of the O_2 molecule (∼4.8 eV). This is, indeed, the case for N = 1 → N = 3 and N = 2 → N = 4 transitions. However, it is not the case for N = 3. Taking into account that, according to earlier studies,[50] MgO surface binds O atoms with the energy of as high as 1.8 eV, oxygen atoms are unlikely to be readily available. Therefore, configurations with N = 3 and a sulfur oxidation state below +6 can remain stable even in the presence of O_2. Configurations of SO_x complexes near 4-coordinated sites are shown in the bottom panel of Figure 4. Their local atomic structures are similar to those found for the 3-coordinated site, with the exception of N = 3, where the local structure of SO_x is determined by the site symmetry. Interestingly, the energy gain due to attachment of a single O atom is comparable to the binding energy of a neutral O atom at the surface and only the N = 2 → N = 4 transition is thermodynamically feasible with respect to splitting of an O_2 molecule. This suggests that $(SO_4)^{2-}$ at the 4-coordinated site can be formed only if the precursor state is formed by an SO_2 molecule displacing an edge O atom. However, given that these SO_x configurations are less stable than those near an oxygen corner, we expect that the relative weight of the SO_x at the edges is insignificant.

3.4. FT-IR Spectroscopy. Fourier transform infrared (FT-IR) spectroscopy is particularly well suited to study sulfur containing surface adsorbates on alkaline earth oxides[17,51] and was employed to complement respective XPS measurements. After annealing and high temperature oxidation, the spectral range between 1000 and 1350 cm^{-1} in the transmission FT-IR spectra of MgO and MgO:SO_x nanocube powders exhibit significant differences (Figure 5a). The MgO:SO_x sample exhibits three intense absorption bands at 1003, 1062, and 1326 cm^{-1} (Figure 5c). Absorptions of lower intensity are observed at 1052, 1086, and 1309 cm^{-1}. Both samples show IR absorption bands at 3720 and 3707 cm^{-1} (Figure 5b). These are attributed to isolated hydroxyl groups which result from

dx.doi.org/10.1021/jp401432j | J. Phys. Chem. C 2013, 117, 7727−7735

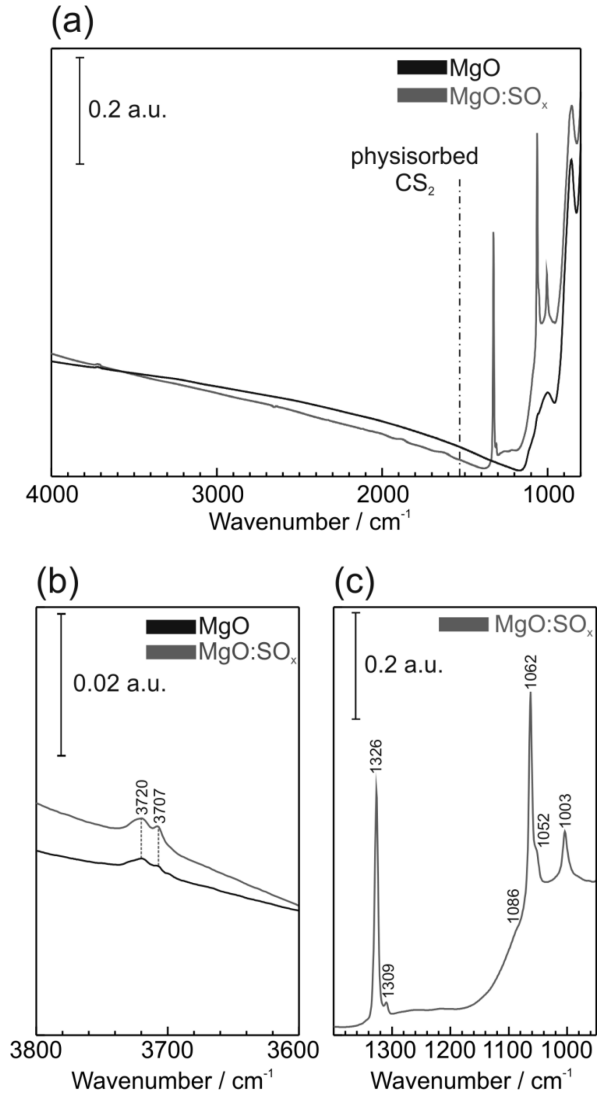

Figure 5. Transmission FT-IR spectra of MgO and MgO:SO_x nanocube powders. Wavenumber ranges from (a) 4000 to 800 cm^{-1}, (b) 3800 to 3600 cm^{-1} specific for hydroxyl groups on MgO, and (c) 1400 to 800 cm^{-1}, a region where absorption bands of $(SO_x)^{2-}$ groups are expected, are shown. The spectra were acquired at room temperature and at a base pressure better than 10^{-5} mbar.

incomplete surface dehydroxylation.[52] It was demonstrated in a recent study[24] that hydroxyl groups absorbing in this wavenumber range can be linked to photoluminescence emission features around 2.9 eV (see also below). Identical positions of the OH stretching vibrations and their comparable intensities indicate that CS_2 adsorption on MgO followed by vacuum annealing and high temperature oxidation affects neither the nature nor the abundance of surface hydroxyls of highest thermal stability.[24]

The infrared absorption band associated with CS_2 molecules in the gas phase are reported to be at 1533 cm^{-1}. Upon physisorption, it shifts to 1525 cm^{-1}.[12] Chemisorbed $[OCS_2]^{2-}$ and $[OCOS]^{2-}$ species absorb at 1125−1025 and 1480 cm^{-1}, respectively, and decompose above room temperature.[12] The IR absorptions in the range 1000−1350 cm^{-1} (Figure 5c) are attributed to SO_x species which remain chemisorbed at MgO nanocubes surfaces (Figure 5c) and exhibit enhanced thermal stability. This is consistent with earlier studies of the interaction of SO_2 with transition metals[53] and metal oxides,[1,3,54−57] as well as that of $(SO_4)^{2-}$ with metal cations in solution.[58] Schoonheydt et al.[59] and Schneider et al.[60] investigated infrared absorption properties of SO_2 adsorbed on MgO. Absorption bands in the region 950−1400 cm^{-1} (Figure 5c) are attributed to sulfite $(SO_3)^{2-}$ and sulfate $(SO_4)^{2-}$ groups. Because of similar IR band positions for both types of adsorbates with their mono- or multidentate bonding character a clear and unambiguous discrimination between them is impossible on the basis of the experimental data presented.[55] The presence of sulfur in a positive oxidation state, however, was confirmed with XPS and is further strengthened by FT-IR spectroscopy.

The assignment of the IR features is corroborated by our ab initio calculations. Vibrational frequencies associated with the SO_x species have been determined for the most stable configurations found for each of the oxidation states of the S species (see Figure 4). In each case, the dynamics matrix has been constructed using numerical differentiation of the total energy with respect to the Cartesian coordinates of the S atoms and their nearest O atom neighbors. The results of these calculations are summarized in Figure 6. In the case of the S^{2-} oxidation state, no vibrational frequencies above 700 cm^{-1} has been detected. As the sulfur oxidation state increases, higher frequency bands appear at ∼850 cm^{-1} for S^{2+} and ∼950 cm^{-1} for S^{4+}. However, vibrational modes with frequencies exceeding 1000 cm^{-1}, observed experimentally (see Figure 5c), appear only in the case of the S^{6+} oxidation states, which reinforces our conclusions that surface sulfur species have positive oxidation states. However, this does not rule out the possibility that a minor contribution of only partially oxidized sulfur species such as S^{4+} in SO_3 groups can be present at the surface as well.

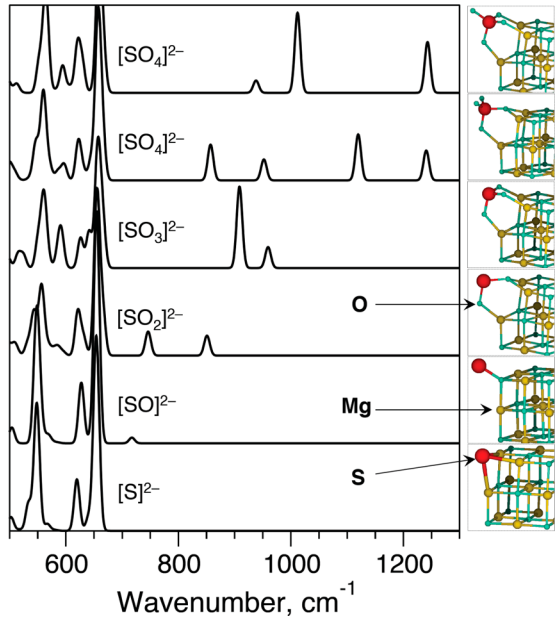

Figure 6. Vibrational spectra (left) and the corresponding local atomic structures (right, see also Figure 4) calculated for the most stable configurations of the surface corner SO_x species for the sulfur oxidation state varying from −2 to +6. The two top spectra are for the most stable (top) and the second most stable (2nd from the top) configurations of $[SO_4]^{2-}$.

3.5. Optical Properties. Since changes in the UV diffuse reflectance of powders of MgO nanocubes are indicative of chemical transformations of the surface elements having the

dx.doi.org/10.1021/jp401432j | J. Phys. Chem. C 2013, 117, 7727−7735

lowest coordination number, we employed this technique to explore the surface electronic structure of MgO:SO_x powders (Figure 7a). For MgO nanocubes absorption bands at 4.6, 5.2, and 5.8 eV correspond to charge transfer excitations at corners, edges, and terrace elements (Figure 6, gray curve).[16,61] For MgO:SO_x powders, the structure of the absorption spectrum is changed (Figure 7a, gray curve) and reveals new bands at 4.0, 5.0, and 5.8 eV.

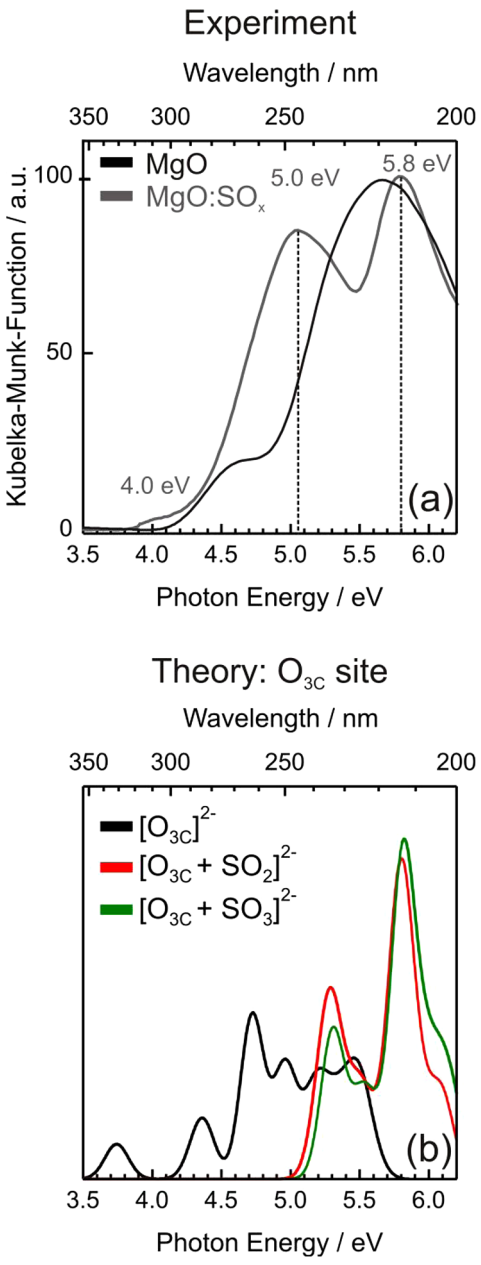

Figure 7. (a) UV diffuse reflectance spectra of MgO and MgO:SO_x nanocubes powders. Measurements were carried out in oxygen atmosphere (p = 10 mbar O_2) and at T = 298 K. (b) Calculated optical absorption spectra.

The low-energy parts of the optical absorption spectra, calculated for the O_{3C}-terminated MgO corner and for the most stable $[SO_3]^{2-}$ and $[SO_4]^{2-}$ species at this corner, are shown in Figure 7b. In all three cases, these parts of the spectra are attributed to the transitions between several highest occupied states (the highest one being HOMO) of the MgO valence band (VB) and a single lowest unoccupied state (LUMO), some of which are shown in Figure 8. It is clear that the

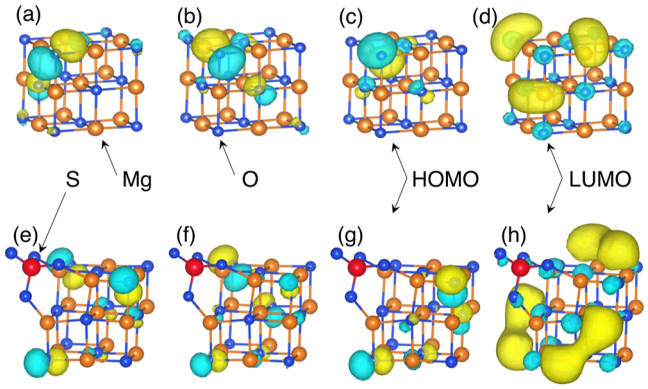

Figure 8. Molecular orbitals involved into the lowest energy optical transitions at MgO corners terminated with: an O^{2-} ion (a–d) and $[SO_4]^{2-}$ molecular ion (e–h).

adsorption features found in pure MgO in the range of 3.7–5.0 eV vanish upon formation of the sulfites and sulfates and, instead, two characteristic peaks at ~5.3 and ~5.9 eV appear. The 5.3 eV peak is associated with the VB states dominated by the 2p atomic states of the O_{4C} atoms that are perpendicular to the (001) edges of the nanocubes (see Figure 8e–g), while the peak at 5.9 eV is dominated by the 2p states that are parallel either to these edges or to (001) atomic planes.

Sulfur oxide moieties are expected to determine the electronic transitions associated with O^{2-} anions in different surface elements. While previous work tentatively assigned the absorption band around 4.2 eV to a charge transfer excitation, which involves S^{2-} and Mg^{2+} in 4-fold coordinated sites,[12] we have to rule out such an assignment for the present case since our XPS results reveal clearly the absence of S^{2-} containing surface elements (Figure 3).

Analysis of the molecular orbitals (MOs) involved in the lowest-energy optical transitions reveals how formation of the corner $(SO_4)^{2-}$ complexes affects the electronic structure of the MgO nanoparticles and, therefore, their optical properties. We highlight two main effects. First, the three highest occupied MOs (shown in Figure 8a–c), which are dominated by the O_{3C} ions in pure MgO, are eliminated once the corner $[SO_4]^{2-}$ complex is formed. Consequently, the highest occupied MOs are associated with the O_{4C} ions next to the corner site (see Figure 8e–g). Second, the lowest unoccupied MO, which is dominated by the Mg_{4C} ions immediately next to the O_{3C} site in pure MgO (see Figure 8d), is so strongly perturbed by the $[SO_4]^{2-}$ complex, that it effectively disappears and the LUMO becomes dominated by the 5-coordinated Mg ions [Figure 8h]. Both of these effects lead to the larger HOMO–LUMO gap in the sulfur-treated MgO and the shift of the lowest optical features, as shown in Figure 7b. We note that this modification of the optical absorption spectrum is different from that reported earlier for the protonated MgO nanocubes.[24] While protons bound to the O_{3C} ions do eliminate the 2p contribution of these oxygens to the top of the valence band, they also shift the LUMO state to the lower energies and, thus, leave the HOMO–LUMO gap almost unaffected.

The PL emission spectrum of MgO nanocubes shows two closely spaced emission bands at $h\nu_{EM}$ = 3.2 eV and $h\nu_{EM}$ = 3.4 eV, which result from the excitation of oxygen-terminated

dx.doi.org/10.1021/jp401432j | J. Phys. Chem. C 2013, 117, 7727–7735

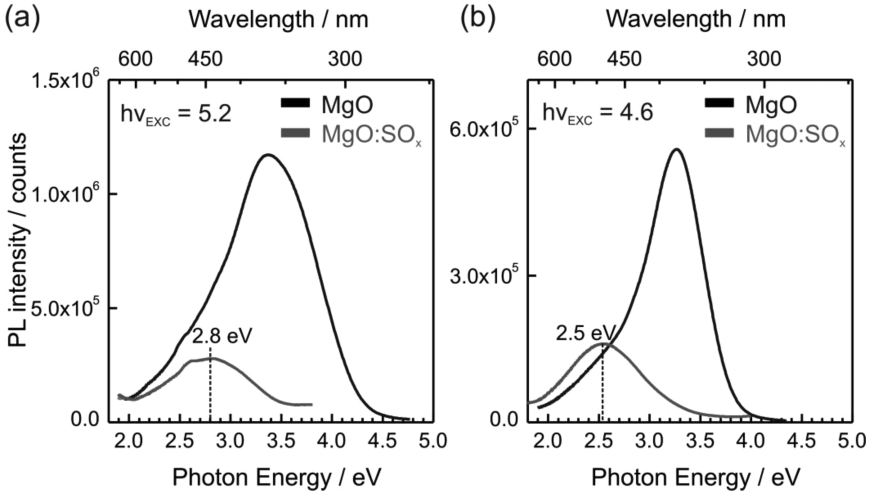

Figure 9. Photoluminescence emission spectra of MgO nanocubes and MgO:SO_x powders using energies of (a) hν = 5.2 eV and (b) hν = 4.6 eV to excite four-coordinated surface O_{4C}^{2-} anions in edges and oxygen-terminated corners in pure MgO. Measurements are carried out at T = 298 K and $p < 5 \times 10^{-6}$ mbar.

corners (O_{3C}^{2-}, hν_{EXC} = 4.6 eV) and surface O_{4C}^{2-} anions in edges (hν_{EXC} = 5.2 eV), respectively (Figure 9, black curves).[27] For MgO:SO_x samples, however, profound changes in the PL emission properties are observed (Figure 9, gray curves). Only significantly less intense emission features at 2.8 and 2.5 eV are observed upon excitation of MgO nanocube edges (hν_{EXC} = 5.2 eV) and corners (hν_{EXC} = 4.6 eV), respectively (Figure 9, gray curves). These emission features are attributed to changes in the surface electronic structure that results from residual surface hydroxyls, which, in turn, were observed by FT-IR spectroscopy (Figure 5c).[24] From the composite PL spectra in Figure 9, we, however, conclude that the majority of relevant PL emission sites are dehydroxylated and give either rise to the PL emission features with maxima at 3.2 and 3.4 eV (MgO, black lines), or not (MgO:SOx, gray lines).

The absence of the emission bands at hν = 3.2 and 3.4 eV is in line with observed changes in the UV diffuse reflectance spectra. Thus, surface sulfites and sulfates effectively extinguish MgO specific PL emissions related to the radiative deactivation of surface excitons at unperturbed corners.[28] Moreover, since all emission bands observed on MgO and MgO:SO_x nanocube powders are perfectly quenched by gaseous oxygen, we conclude that corresponding excitation and subsequent radiative deactivation processes originate exclusively from the surface excited states. This evidence provides strong support for the conclusion that MgO nanocube corners were functionalized with surface SO_x species.

The results presented here advance our understanding of sulfur oxide adsorption on mineral surfaces,[1,3,62] as well as suggest strategies that aim at the control over surface acidity of metal oxide catalysts via sulfatation.[63] Due to a variety of potential applications for highly dispersed alkaline earth oxides with intrinsic and extrinsic surface functionalities it is necessary to further develop our research on structure−property relationships. Moreover, related insights are indispensable for the knowledge-based functionalization of metal oxide nanoparticle powders in general. Surface sulfur oxides are promising anchor groups for coupling reactions[64] that may link metal oxide nanocubes to other objects, such as nanoparticles, two-dimensional substrates, and porous hosts. We believe that the here presented approach provides a well-defined starting point for inte gration of nanoscale building blocks into higher order assemblies. The opportunity to track the underlying transformation process with different spectroscopic techniques in conjunction with ab initio calculations provides a firm base for future control over the optolectronic properties.

4. SUMMARY

Structure, morphology, and surface optical properties of MgO nanocubes with surface sulfites and sulfates were studied experimentally and using ab initio calculations. XRD and TEM reveal that the rock salt structure and the cubic particle morphology of MgO nanocubes remain unaltered upon CS_2 adsorption and subsequent oxidation and vacuum annealing. XPS and IR spectroscopy results point to the fact that following this sample treatment MgO surfaces become decorated with $(SO_3)^{2-}$ or $(SO_4)^{2-}$ groups that are thermally stable up to 1173 K. Respective surface decorations are associated with profound changes in the UV diffuse reflectance properties. In addition, the extinction of MgO specific photoluminescence properties which can be interrogated by excitation of edges (hν_{EXC} = 5.2 eV) and corners (hν_{EXC} = 4.6 eV) clearly shows that the surface sites involved in excitation−emission processes on pure MgO are completely modified by sulfur-containing groups.

AUTHOR INFORMATION

Corresponding Author

*E-mail: oliver.diwald@sbg.ac.at (O.D.); p.sushko@ucl.ac.uk (P.V.S).

Notes

The authors declare no competing financial interest.

ACKNOWLEDGMENTS

The authors gratefully acknowledge the support of the German Research Foundation (DFG), which, within the framework of its “Excellence Initiative”, supports the Cluster of Excellence “Engineering of Advanced Materials” at the University of Erlangen-Nuremberg. Part of the support stems from the Fonds zur Förderung der Wissenschaftlichen Forschung (Grant FWF-P19848-N20), which is also gratefully acknowledged. P.V.S. is supported by the Royal Society and MEXT Elements Science

and Technology Project. This work was carried out within the COST action D41 Inorganic Oxides.

REFERENCES

(1) Stark, J. V.; Park, D. G.; Lagadic, I.; Klabunde, K. J. Nanoscale Metal Oxide Particles/Clusters as Chemical Reagents. Unique Surface Chemistry on Magnesium Oxide As Shown by Enhanced Adsorption of Acid Gases (Sulfur Dioxide and Carbon Dioxide) and Pressure Dependence. *Chem. Mater.* **1996**, *8* (8), 1904−1912.

(2) Liu, C.; Ma, Q.; Liu, Y.; Ma, J.; He, H. Synergistic Reaction between SO_2 and NO_2 on Mineral Oxides: A Potential Formation Pathway of Sulfate Aerosol. *Phys. Chem. Chem. Phys.* **2012**, *14* (5), 1668−1676.

(3) Usher, C. R.; Michel, A. E.; Grassian, V. H. Reactions on Mineral Dust. *Chem. Rev.* **2003**, *103* (12), 4883−4940.

(4) Schneider, W. F. Qualitative Differences in the Adsorption Chemistry of Acidic (CO_2, SO_x) and Amphiphilic (NO_x) Species on the Alkaline Earth Oxides. *J. Phys. Chem. B* **2004**, *108* (1), 273−282.

(5) Livraghi, S.; Paganini, M.; Chiesa, M.; Giamello, E. Reduction and Fragmentation of CS_2 at the Surface of Electron-Rich MgO: An EPR Study. *Res. Chem. Intermed.* **2006**, *32* (8), 777−786.

(6) Aydin, C.; Kulkarni, A.; Chi, M.; Browning, N. D.; Gates, B. C. Atomically Resolved Site-Isolated Catalyst on MgO: Mononuclear Osmium Dicarbonyls Formed from $Os_3(CO)_{12}$. *J. Phys. Chem. Lett.* **2012**, *3* (14), 1865−1871.

(7) Sternig, A.; Stankic, S.; Mueller, M.; Bernardi, J.; Knoezinger, E.; Diwald, O. Photoluminescent Nanoparticle Surfaces: the Potential of Alkaline Earth Oxides for optical Applications. *Adv. Mater. (Weinheim, Ger.)* **2008**, *20* (24), 4840−4844.

(8) Chiesa, M.; Paganini, M. C.; Giamello, E. Bidimensional Solvation and Delocalisation of Electrons at the Surface of an Insulating Oxide: The Role of Surface Hydroxyl Groups on MgO. *ChemPhysChem.* **2004**, *5* (12), 1897−1900.

(9) Yoshida, H.; Tanaka, T.; Funabiki, T.; Yoshida, S. Photoluminescence Spectra resulting from Hydroxy Groups on Magnesium Oxide supported on Silica. *J. Chem. Soc., Faraday Trans.* **1994**, *90* (14), 2107−2111.

(10) Bai, Y.; Buchner, F.; Kellner, I.; Schmid, M.; Vollnhals, F.; Steinrück, H.-P.; Marbach, H.; Gottfried, J. M. Adsorption of Cobalt(II) Octaethylporphyrin and 2*H*-Octaethylporphyrin on Ag(111): New Insight into the Surface Coordinative Bond. *New J. Phys.* **2009**, *11* (12), 125004.

(11) Kulkarni, A.; Lobo-Lapidus, R. J.; Gates, B. C. Metal Clusters on Supports: Synthesis, Structure, Reactivity, and Catalytic Properties. *Chem. Commun.* **2010**, *46* (33), 5997.

(12) Scarano, D.; Bertarione, S.; Zecchina, A.; Soave, R.; Pacchioni, G. Adsorption of CS_2 on MgO Microcrystals: Formation of a S-Doped MgO Surface. *Phys. Chem. Chem. Phys.* **2002**, *4* (2), 366−374.

(13) Audi, A. A.; Sherwood, P. M. A. X-ray Photoelectron Spectroscopic Studies of Sulfates and Bisulfates interpreted by X band band Structure Calculations. *Surf. Interface Anal.* **2000**, *29* (4), 265−275.

(14) Tsuji, H.; Hattori, H. Oxide Surfaces that Catalyse an Acid−Base Reaction with Surface Lattice Oxygen Exchange: Evidence of Nucleophilicity of Oxide Surfaces. *ChemPhysChem* **2004**, *5* (5), 733−736.

(15) Tsuji, H.; Okamura-Yoshida, A.; Shishido, T.; Hattori, H. Dynamic Behavior of Carbonate Species on Metal Oxide Surface: Oxygen Scrambling between Adsorbed Carbon Dioxide and Oxide Surface. *Langmuir* **2003**, *19* (21), 8793−8800.

(16) Stankic, S.; Mueller, M.; Diwald, O.; Sterrer, M.; Knoezinger, E.; Bernardi, J. Size-Dependent Optical Properties of MgO Nanocubes. *Angew. Chem., Int. Ed.* **2005**, *44* (31), 4917−4920.

(17) Spoto, G.; Gribov, E. N.; Ricchiardi, G.; Damin, A.; Scarano, D.; Bordiga, S.; Lamberti, C.; Zecchina, A. Carbon Monoxide on MgO from Dispersed Solids to Single Crystals: A Review and New Advances. *Prog. Surf. Sci.* **2004**, *76* (3−5), 71−146.

(18) Stankic, S.; Sterrer, M.; Hofmann, P.; Bernardi, J.; Diwald, O.; Knoezinger, E. Novel Optical Surface Properties of Ca^{2+}-Doped MgO Nanocrystals. *Nano Lett.* **2005**, *5* (10), 1889−1893.

(19) Chiesa, M.; Giamello, E.; Annino, G.; Massa, C. A.; Murphy, D. M. Multifrequency High-Field EPR Study of (H+)(e−) Pairs Localized at the Surface of Polycrystalline MgO. *Chem. Phys. Lett.* **2007**, *438* (4−6), 285−289.

(20) Chiesa, M.; Paganini, M. C.; Giamello, E.; Di Valentin, C.; Pacchioni, G. First Evidence of a Single-Ion Electron Trap at the Surface of an Ionic Oxide. *Angew. Chem., Int. Ed.* **2003**, *42* (15), 1759−1761.

(21) Bailly, M.-L.; Costentin, G.; Lauron-Pernot, H.; Krafft, J. M.; Che, M. Physicochemical and in Situ Photoluminescence Study of the Reversible Transformation of Oxide Ions of Low Coordination into Hydroxyl Groups upon Interaction of Water and Methanol with MgO: The Journal of Physical Chemistry B. *J. Phys. Chem. B* **2004**, *109* (6), 2404−2413.

(22) McKenna, K. P.; Sushko, P. V.; Shluger, A. L. Inside Powders: A Theoretical Model of Interfaces between MgO Nanocrystallites. *J. Am. Chem. Soc.* **2007**, *129* (27), 8600−8608.

(23) McKenna, K. P.; Koller, D.; Sternig, A.; Siedl, N.; Govind, N.; Sushko, P. V.; Diwald, O. Optical Properties of Nanocrystal Interfaces in Compressed MgO Nanopowders. *ACS Nano* **2011**, *5* (4), 3003−3009.

(24) Mueller, M.; Stankic, S.; Diwald, O.; Knoezinger, E.; Sushko, P. V.; Trevisanutto, P. E.; Shluger, A. L. Effect of Protons on the Optical Properties of Oxide Nanostructures. *J. Am. Chem. Soc.* **2007**, *129* (41), 12491−12496.

(25) Sushko, P. V.; Gavartin, J. L.; Shluger, A. L. Electronic Properties of Structural Defects at the MgO (001) Surface. *J. Phys. Chem. B* **2002**, *106* (9), 2269−2276.

(26) Shluger, A. L.; Sushko, P. V.; Kantorovich, L. N. Spectroscopy of Low-Coordinated Surface Sites: Theoretical Study of MgO. *Phys. Rev. B: Condens. Matter Mater. Phys.* **1999**, *59* (3), 2417−2430.

(27) Sternig, A.; Mueller, M.; McCallum, M.; Bernardi, J.; Diwald, O. BaO Clusters on MgO Nanocubes. A Quantitative Analysis of Optical Powder Properties. *Small* **2010**, *6* (4), 582−588.

(28) Sternig, A.; Stankic, S.; Müller, M.; Siedl, N.; Diwald, O. Surface Exciton Separation in Photoexcited MgO Nanocube Powders. *Nanoscale* **2012**, *4* (23), 7494−7500.

(29) Shaikhutdinov, S.; Freund, H. J. Ultrathin Oxide Films on Metal Supports: Structure−Reactivity Relations: Annual Review of Physical Chemistry. *Annu. Rev. Phys. Chem.* **2012**, *63* (1), 619−633.

(30) Happel, M.; Mysliveček, J.; Johánek, V.; Dvořák, F.; Stetsovych, O.; Lykhach, Y.; Matolín, V.; Libuda, J. Adsorption Sites, Metal−Support Interactions, and Oxygen Spillover Identified by Vibrational Spectroscopy of Adsorbed CO: A Model Study on Pt/Ceria Catalysts. *J. Catal.* **2012**, *289* (0), 118−126.

(31) Weilach, C.; Spiel, C.; Föttinger, K.; Rupprechter, G. Carbonate Formation on Al_2O_3 Thin Film Model Catalyst Supports. *Surf. Sci.* **2011**, *605* (15−16), 1503−1509.

(32) Scheiber, P.; Riss, A.; Schmid, M.; Varga, P.; Diebold, U. Observation and Destruction of an Elusive Adsorbate with STM: O_2/TiO2(110). *Phys. Rev. Lett.* **2010**, *105* (21), No. 216101.

(33) Batzill, M.; Diebold, U. Surface Studies of Gas Sensing Metal Oxides. *Phys. Chem. Chem. Phys.* **2007**, *9* (19), 2307−2318.

(34) Sterrer, M.; Risse, T.; Freund, H.-J. Low Temperature Infrared Spectra of CO Adsorbed on the Surface of MgO Thin Films. *Surf. Sci.* **2005**, *596* (1−3), 222−228.

(35) Knoezinger, E.; Jacob, K. H.; Singh, S.; Hofmann, P. Hydroxyl Groups as IR Active Surface Probes on MgO Crystallites. *Surf. Sci.* **1993**, *290* (3), 388−402.

(36) The vapor pressure of CS_2 is approximately 400 mbar at 293 K.

(37) Moulder, J. F.; Chastain, J. *Handbook of X-ray Photoelectron Spectroscopy. A Reference Book of Standard Spectra for Identification and Interpretation of XPS Data*; Physical Electronics Division, Perkin-Elmer Corp.: Eden Prairie, MN, 1992.

(38) Seah, M. P.; Briggs, D. *Practical Surface Analysis*, 2nd ed.; Wiley: Chichester, U.K., 1995.

(39) National Institute of Standards and Technology, Gaithersburg. NIST X-ray Photoelectron Spectroscopy Database. http://srdata.nist.gov/xps/.
(40) Wadt, W. R.; Hay, P. J. Ab Initio Effective Core Potentials for molecular Calculations. Potentials for Main Group Elements Na to Bi. *J. Chem. Phys.* **1985**, *82* (1), 284.
(41) Sushko, P. V.; Shluger, A. L.; Catlow, C. R. A. Relative Energies of Surface and Defect States: Ab Initio Calculations for the MgO (001) Surface. *Surf. Sci.* **2000**, *450* (3), 153−170.
(42) Muñoz Ramo, D.; Sushko, P.; Gavartin, J.; Shluger, A. Oxygen Vacancies in Cubic ZrO_2 Nanocrystals Studied by an Ab Initio Embedded Cluster Method. *Phys. Rev. B* **2008**, *78* (23), No. 235432.
(43) Becke, A. D. Density-Functional Thermochemistry. III. The Role of Exact Exchange. *J. Chem. Phys.* **1993**, *98* (7), 5648−5652.
(44) Lee, C.; Yang, W.; Parr, R. G. Development of the Colle−Salvetti Correlation−Energy Formula into a Functional of the Electron Density. *Phys. Rev. B: Condens. Matter Mater. Phys.* **1988**, *37* (2), 785−789.
(45) Frisch, M. J.; Trucks, G. W.; Schlegel, H. B.; Scuseria, G. E.; Robb, M. A.; Cheeseman, J. R.; Montgomery, J. A., Jr.; Vreven, T.; Kudin, K. N.; Burant, J. C.; Millam, J. M.; Iyengar, S. S.; Tomasi, J.; Barone, V.; Mennucci, B.; Cossi, M.; Scalmani, G.; Rega, N.; Petersson, G. A.; Nakatsuji, H.; Hada, M.; Ehara, M.; Toyota, K.; Fukuda, R.; Hasegawa, J.; Ishida, M.; Nakajima, T.; Honda, Y.; Kitao, O.; Nakai, H.; Klene, M.; Li, X.; Knox, J. E.; Hratchian, H. P.; Cross, J. B.; Bakken, V.; Adamo, C.; Jaramillo, J.; Gomperts, R.; Stratmann, R. E.; Yazyev, O.; Austin, A. J.; Cammi, R.; Pomelli, C.; Ochterski, J. W.; Ayala, P. Y.; Morokuma, K.; Voth, G. A.; Salvador, P.; Dannenberg, J. J.; Zakrzewski, V. G.; Dapprich, S.; Daniels, A. D.; Strain, M. C.; Farkas, O.; Malick, D. K.; Rabuck, A. D.; Raghavachari, K.; Foresman, J. B.; Ortiz, J. V.; Cui, Q.; Baboul, A. G.; Clifford, S.; Cioslowski, J.; Stefanov, B. B.; Liu, G.; Liashenko, A.; Piskorz, P.; Komaromi, I.; Martin, R. L.; Fox, D. J.; Keith, T.; Al-Laham, M. A.; Peng, C. Y.; Nanayakkara, A.; Challacombe, M.; Gill, P. M. W.; Johnson, B.; Chen, W.; Wong, M. W.; Gonzalez, C.; Pople, J. A. *Gaussian 03*, revision B.04; Gaussian, Inc.: Wallingford, CT, 2003.
(46) Bauernschmitt, R.; Ahlrichs, R. Treatment of Electronic Excitations within the Adiabatic Approximation of Time Dependent Density Functional Theory. *Chem. Phys. Lett.* **1996**, *256* (4−5), 454−464.
(47) Scherrer, P. Röntgendiffraktion, Halbwertsbreiten. *Goett. Nachr.* **1918**, No. *2*, 98−100.
(48) Weidenthaler, C. Pitfalls in the Characterization of Nanoporous and Nanosized Materials. *Nanoscale* **2011**, *3* (3), 792−810.
(49) Ding, Y.; Zhang, G.; Zhang, S.; Huang, X.; Yu, W.; Qian, Y. Preparation and Characterization of Magnesium Hydroxide Sulfate Hydrate Whiskers: Chemistry of Materials. *Chem. Mater.* **2000**, *12* (10), 2845−2852.
(50) Kantorovich, L.; Gillan, M. Adsorption of Atomic and Molecular Oxygen on the MgO (001) Surface. *Surf. Sci.* **1997**, *374* (1−3), 373−386.
(51) Spoto, G.; Bordiga, S.; Zecchina, A.; Cocina, D.; Gribov, E. N.; Regli, L.; Groppo, E.; Lamberti, C. New Frontier in Transmission IR Spectroscopy of Molecules Adsorbed on High Surface Area Solids: Experiments below Liquid Nitrogen Temperature: Recent Advances in In Situ and Operando Studies of Catalytic Reactions. *Catal. Today* **2006**, *113* (1−2), 65−80.
(52) Diwald, O.; Sterrer, M.; Knoezinger, E. Site Selective Hydroxylation of the MgO Surface. *Phys. Chem. Chem. Phys.* **2002**, *4* (12), 2811−2817.
(53) Lin, X.; Schneider, W. F.; Trout, B. L. Chemistry of Sulfur Oxides on Transition Metals. II. Thermodynamics of Sulfur Oxides on Platinum(111). *J. Phys. Chem. B* **2003**, *108* (1), 250−264.
(54) Goodsel, A. J.; Low, M. J. D.; Takezawa, N. Reactions of Gaseous Pollutants with Solids. II. Infrared Study of Sorption of Sulfur Dioxide on Magnesium Oxide. *Environ. Sci. Technol.* **1972**, *6* (3), 268−273.
(55) Happel, M.; Desikusumastuti, A.; Sobota, M.; Laurin, M.; Libuda, J. Impact of Sulfur Poisoning on the NOx Uptake of a NOx Storage and Reduction (NSR) Model Catalyst. *J. Phys. Chem. C* **2010**, *114* (10), 4568−4575.
(56) Luckas, N.; Viñes, F.; Happel, M.; Desikusumastuti, A.; Libuda, J.; Görling, A. Density Functional Calculations and IR Reflection Absorption Spectroscopy on the Interaction of SO_2 with Oxide-Supported Pd Nanoparticles. *J. Phys. Chem. C* **2010**, *114* (32), 13813−13824.
(57) Zorn, K.; Föttinger, K.; Halwax, E.; Vinek, H. Active Sites on Pt-Containing Sulfated Zirconia. *Top. Catal* **2007**, *46* (1−2), 93−100.
(58) Lefèvre, G. In Situ Fourier-Transform Infrared Spectroscopy Studies of Inorganic Ions Adsorption on Metal Oxides and Hydroxides. *Adv. Colloid Interface Sci.* **2004**, *107* (2−3), 109−123.
(59) Schoonheydt, R. A.; Lunsford, J. H. Infrared Spectroscopic Investigation of the Adsorption and Reactions of SO_2 on MgO. *J. Catal.* **1972**, *26* (2), 261−271.
(60) Schneider, W. F.; Li, J.; Hass, K. C. Combined Computational and Experimental Investigation of SOx Adsorption on MgO. *J. Phys. Chem. B* **2001**, *105* (29), 6972−6979.
(61) Sternig, A.; Koller, D.; Siedl, N.; Diwald, O.; McKenna, K. Exciton Formation at Solid−Solid Interfaces: A Systematic Experimental and Ab Initio Study on Compressed MgO Nanopowders. *J. Phys. Chem. C* **2012**, *116* (18), 10103−10112.
(62) Goodman, A. L.; Li, P.; Usher, C. R.; Grassian, V. H. Heterogeneous Uptake of Sulfur Dioxide On Aluminum and Magnesium Oxide Particles. *J. Phys. Chem. A* **2001**, *105* (25), 6109−6120.
(63) Song, X.; Sayari, A. Sulfated Zirconia-Based Strong Solid-Acid Catalysts: Recent Progress. *Catal. Rev.* **1996**, *38* (3), 329−412.
(64) Park, H.; Afzali, A.; Han, S.-J.; Tulevski, G. S.; Franklin, A. D.; Tersoff, J.; Hannon, J. B.; Haensch, W. High-Density Integration of Carbon Nanotubes via Chemical Self-Assembly. *Nat. Nanotechnol.* **2012**, *7*, 787−791.